Journal of Colloid and Interface Science 348 (2010) 167–176

Contents lists available at ScienceDirect

Journal of Colloid and Interface Science

www.elsevier.com/locate/jcis

Adsorption of sodium dodecyl sulfate (SDS) at ZnSe and α-Fe_2O_3 surfaces: Combining infrared spectroscopy and batch uptake studies

Xiaodong Gao, Jon Chorover *

Department of Soil, Water, and Environmental Science, University of Arizona, Tucson, AZ 85721, USA

ARTICLE INFO

Article history:
Received 18 February 2010
Accepted 7 April 2010
Available online 13 April 2010

Keywords:
SDS
Adsorption
Hematite
ZnSe IRE
ATR–FTIR spectroscopy

ABSTRACT

Adsorption of sodium dodecyl sulfate (SDS) at the solid/aqueous interface was examined as a function of pH and SDS concentration ([SDS]) using attenuated total reflectance–Fourier transform infrared (ATR–FTIR) spectroscopy and batch uptake experiments. Two types of sorbent surfaces were compared: (i) a hydrophobic zinc selenide (ZnSe) ATR internal reflection element (IRE) and (ii) the same surface coated with hydrophilic nanoparticulate α-Fe_2O_3 (hematite). The results indicate that adsorption to the ZnSe IRE is affected by both electrostatic attraction and hydrophobic interaction. Batch adsorption and ATR–FTIR spectral results are consistent with SDS forming outer-sphere complexes at the α-Fe_2O_3 surface. There is also no evidence for ligand (SDS)-promoted dissolution of hematite. Adsorption to hematite is dominated by anion exchange and surfactant self-assembly. ATR–FTIR data indicate that adsorption to both surfaces shows a strong pH dependence at low [SDS] and negligible pH dependence when [SDS] exceeds the critical micelle concentration (cmc). Adsorption to ZnSe IRE shows small variation with [SDS], apparently due to a lack of surfactant self-assembly at the interface. Adsorption to α-Fe_2O_3 is a rapid process; equilibrium is reached within a few minutes. Conversely, adsorption to the ZnSe IRE shows strong longer time dependence; evidently, hydrophobic interfacial reactions constitute a much slower process.

Published by Elsevier Inc.

1. Introduction

Ionic surfactants are a class of organic compounds that contain both hydrophobic (tail) and hydrophilic (head) groups in each molecule. Those that are naturally produced by microorganisms [1] or plants [2] are termed biosurfactants. A variety of synthetic surfactants that are widely used in many industries can also be found as contaminants in surface water and soils [3]. The ubiquitous presence of surfactants in the environment plays an important role in many processes at biogeochemical interfaces, including those that control the fate and transport of organic contaminants [3], colloidal stability [4], and ligand-controlled mineral dissolution [5,6]. SDS is a common, synthetic anionic surfactant that is widely used in many cleaning and hygiene products. The SDS molecule contains a 12 carbon saturated alkyl chain bound to a negatively charged sulfonate head ($-OSO_3^-$) and, therefore, it is structurally comparable to many biosurfactants for which it is also used as a model (Scheme 1).

The extent of adsorption of ionic surfactants from aqueous solution to charged particles (e.g., silica and metal oxides) has been primarily studied using traditional adsorption isotherms and pH edges [4,5,7–10]. These studies suggest that electrostatic forces and surfactant self-assembly are dominant mechanisms governing the sorption processes at most solid/aqueous interfaces. Furthermore, the observation of four distinct regions in log–log plots of adsorption isotherm data has been often interpreted to reflect variation in sorption mechanism driven by surface loading [4–6,11–13]. Briefly, at very low surfactant aqueous concentration (region I), adsorption is considered dominated by electrostatic forces between the hydrophilic head and the solid surface. With increasing concentration (region II), surfactant molecules are thought to form hemimicelle-like, monolayered clusters on the surface that involve lateral hydrophobic interactions between tails of neighboring molecules, giving rise to hydrophobic patches on the surface. In region III, a further increase of the surfactant concentration induces the formation of a more complete bilayer structure (admicelles) on the mineral surface. Finally, a complete bilayer tends to form on the mineral surface when the surfactant solution concentration exceeds the cmc (region IV). Thus, both electrostatic sorbate–adsorbent forces and hydrophobic adsorbate–adsorbate interactions are important in the adsorption process. Admicelle formation is a surface-induced process that can occur well below the cmc of the surfactant in solution [5]. In addition, the presence of background electrolyte can significantly reduce the cmc by shielding the

* Corresponding author. Fax: +1 520 621 1647.
E-mail address: chorover@cals.arizona.edu (J. Chorover).

0021-9797/$ - see front matter Published by Elsevier Inc.
doi:10.1016/j.jcis.2010.04.011

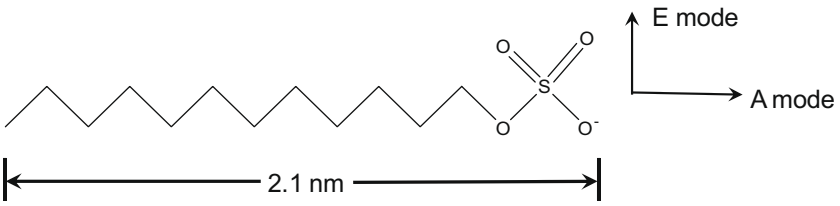

Scheme 1. Chemical structure of sodium dodecyl sulfate (SDS).

electrostatic repulsive forces between charged ionic heads [3]. For example, in the presence of 10 mM background electrolyte, the cmc of SDS decreased from 8.1 to 6.5 mM [12]. Each SDS micelle contains ca. 60 SDS molecules with the radius roughly equal to the length of the hydrocarbon chain (ca. 2.1 nm) [14].

Although considerable attention has been focused on adsorption of ionic surfactants to mineral surfaces, the sorption mechanisms cannot be conclusively determined with macroscopic experiments alone because such experiments do not provide molecular structural information. Recently, a variety of advanced techniques, such as atomic force microscopy (AFM) [15,16], fluorescence quenching [17], and optical reflectometry [12], have become available to study the molecular structure of adsorbed surfactants at solid/aqueous interfaces. These studies provide new insights on surfactant adsorption mechanisms and demonstrate, for example, that surfactants form discrete interfacial aggregates rather than simple uniform monolayers or bilayers.

In situ ATR–FTIR spectroscopy is a surface-sensitive technique that can be used to interrogate the aqueous–adsorbent interface at the molecular scale, thereby providing mechanistic information on adsorption mechanisms. For example, prior ATR–FTIR spectroscopy studies of SO_4^{2-} adsorption to Fe (oxyhydr)oxides indicate that the SO_4^{2-} anion can form either outer-sphere or inner-sphere complexes depending on solution pH, ionic strength, and surface loading [18–20]. In situ ATR–FTIR has also been employed in a few cases to investigate the interfacial reactions of SDS at various mineral surfaces, including Al_2O_3 [21,22], TiO_2 [22,23], and α-Fe_2O_3 [10], but the range of experimental conditions probed was too narrow to facilitate interpretation of adsorption–desorption phenomena. The results of these studies suggest that SDS forms outer-sphere surface complexes, likely involving a combination of electrostatic and hydrophobic interactions. However, the effects of solution chemistry and SDS concentration, which have been shown in other cases to strongly affect adsorption mechanisms, were not systematically examined. In addition, all the adsorbent substrates used in these prior studies were relatively hydrophilic (e.g., Fe and Al oxides). Mechanisms of SDS adsorption to more hydrophobic sorbents, such as humic substances that are ubiquitously present in the environment, remain poorly understood. Hence, there is a strong need for comparative adsorption studies that include more hydrophobic substrates, as well as those that probe the kinetics of SDS adsorption and restructuring in the interfacial region.

In this work, ATR–FTIR was used to investigate the adsorption of SDS on a relatively hydrophobic ZnSe IRE and the same IRE coated with hydrophilic, nanoparticulate hematite (α-Fe_2O_3), as a function of pH and SDS concentration. The dynamic contact angles of H_2O on ZnSe and hematite surfaces were reported at 76.3 and ~42.5°, respectively [24,25]. The spectroscopic data were correlated with batch adsorption experiments to elucidate in situ adsorption mechanisms of SDS on mineral surfaces. By doing so, the study described here addresses a gap in the literature that exists between published works pertaining to systematic, quantitative studies of surfactant adsorption and those that describe spectroscopic analyses of sorption mechanism.

2. Materials and methods

2.1. Colloidal hematite synthesis and characterization

Colloidal hematite was prepared using the method of Schwertmann and Cornell [26]. Briefly, 100 ml of freshly prepared 1 M $Fe(NO_3)_3 \bullet 9H_2O$ (J.T. Baker) solution was added dropwise to 1 L of boiling Barnstead Nanopure (BNP) water during vigorous stirring. After cooling to room temperature, the suspension was transferred into dialysis tubing (Spectra/Por 7, 1000 MWCO) and dialyzed against ultrapure water (replaced twice daily) with pH adjusted to 4.0 using 0.1 M HNO_3 solution. Dialysis was considered complete when pH stabilized at 4.0 (ca. 2 weeks). The colloidal suspension was then transferred to a polyethylene bottle and stored at 4 °C.

Mineralogical composition, particle size, surface area, and electrophoretic mobility of the synthetic hematite were determined by X-ray diffraction (XRD), transmission electron microscopy (Philips FEI CM12 STEM), surface area analyzer (Beckman Coulter SA 3100), and zeta potential analyzer (Brookhaven Instruments ZetaPLAS, NY), respectively. The XRD pattern confirmed the material as pure hematite, and TEM images showed rough spherical particles ca. 10–20 nm in diameter, as published elsewhere [27]. The synthetic hematite has a measured isoelectric point (IEP) of ~7.7–7.8 in 1 mM $NaNO_3$ background electrolyte [27] and a BET N_2 specific surface area of 69.3 ± 0.3 $m^2\ g^{-1}$.

2.2. Batch adsorption envelope and isotherm experiments

Sodium dodecyl sulfate (99%) was purchased from Sigma–Aldrich Co. (St. Louis, MO) and used as received. A series of batch adsorption experiments were carried out over a range of initial SDS concentrations and pH values in 10 mM NaCl background electrolyte for a 24 h reaction time. Solutions of 10 mM HCl or NaOH were used to adjust suspension pH (prior to reaction) to achieve a final pH range of 3.0–9.0 for sorption envelope experiments and pH 6.0 for isotherm experiments. Sorption envelope experiments were carried out at three initial SDS concentrations of 0.1, 1.0, and 10.0 mM, corresponding to the SDS concentrations used for FTIR studies. For isotherm experiments, initial SDS concentrations ranging from 0.01 to 10.0 mM at pH 6 were used. To achieve the desired adsorbent to SDS ratios, 10 ml aliquots of α-Fe_2O_3 suspension in 10 mM NaCl background electrolyte solution were first pipetted into 35 ml polyethylene centrifuge tubes. Five milliliters of 10 mM NaCl solution containing different concentrations of SDS was then introduced to reach the desired final SDS concentration. The final solid concentration of α-Fe_2O_3 was 5.0 g L^{-1}. All samples were wrapped in aluminum foil to prevent photodegradation. The suspensions were equilibrated on an end-over-end shaker (7 rpm) for the desired reaction time. The pH was then remeasured, and samples were centrifuged at 12,812*g* and 25 °C for 30 min. Adsorbent-free controls (no mineral) were reacted concurrently to monitor for any unintended compound loss during the reaction processes.

The supernatant was aspirated and filtered through a 0.2 μm nominal pore size syringe filter. An aliquot of the filtrate was acidified to pH < 2 with trace metal grade HNO_3 for Fe concentration analysis. Total Fe concentration was determined using a Perkin-Elmer Elan DRC II inductively coupled plasma–mass spectrometer (ICP–MS). The dissolved SDS concentration was determined by measuring nonpurgable organic carbon (NPOC) with a total organic carbon analyzer (Shimadzu Model TOC–V_{CSH}) following solution acidification to pH < 2 with HCl. Standards were prepared by dissolving known masses of SDS in the same background electrolyte. The amount of adsorbed SDS was calculated on the basis of loss from solution.

2.3. Hematite coating of IRE surface

To achieve a uniform, thin layer porous film of hematite nanoparticles for ATR–FTIR experiments, 500 μl of the hematite suspension (3.3 g L^{-1}) was evenly deposited onto the IRE surface and allowed to dry in a vacuum oven (10 mm Hg) overnight at room temperature. After drying, the hematite film was gently rinsed with BNP water to remove loosely adhered particles. A new film was prepared for each experiment, and spectra of dry oxide films were collected each time to determine consistency of coating. For the removal of hematite coating, a wet microcloth/cotton (CleanTex) was used to wipe off the particulate film, followed by rinsing with methanol and BNP water.

2.4. Infrared spectroscopy

ATR–FTIR spectroscopy was employed to investigate the adsorption mechanisms as a function of surface chemistry, pH, and SDS concentration. Experiments were conducted at three SDS concentrations (0.1, 1.0, and 10.0 mM) with pH ranging from 3.0 to 9.0 on both the bare ZnSe IRE and hematite-coated surfaces, and in 10 mM NaCl background electrolyte to allow direct comparison with the batch experiments. The SDS concentrations were chosen to probe different regions of the adsorption isotherm, as noted above, and to assess the formation of different sorbate structures at the solid/aqueous interfaces, corresponding to individual molecules, hemimicelle, and admicelle structures, respectively [5,8,10]. For each solution chemistry condition, an aliquot of 500 μl SDS solution was applied directly to the uncoated or hematite coated 45° ZnSe IRE (nine internal reflections, 56 × 10 × 3 mm) (PIKE Technologies, Inc.) in a trough-style sample holder by pipette. A volatile liquid cover was used to prevent solution evaporation during the measurements. To examine the temporal dependence of surface interaction, spectra were recorded as a function of time (0, 15, 30, 60, 90, and 120 min after sample introduction) at room temperature.

Infrared spectra were recorded using a Magna-IR 560 Nicolet spectrometer (Madison, WI) equipped with a CsI beam splitter and a DTGS detector. All spectra were obtained by averaging 400 scans at 4 cm^{-1} resolution over the spectral range of 4000–800 cm^{-1} using the autogain function and aperture set at 100 without ATR correction for wavelength dependence. A final spectrum was obtained by subtracting the appropriate background spectrum from that of the SDS suspension. The dry, clean 45° ZnSe crystal was consistently used for background correction. The spectrometer was continuously purged with CO_2 free air to diminish CO_2 absorbance. Data collection and spectral processes, including subtraction and baseline correction, were performed using the OMNIC program (Thermo Nicolet Co.). Quantitative Lorentzian peak fitting was performed using GRAMS/AI software (Thermo Electron Corp.).

3. Results and discussion

3.1. Quantitative adsorption measurements

3.1.1. SDS adsorption isotherms

Adsorption isotherms for SDS on α-Fe_2O_3 (pH 6.0, 10 mM NaCl background electrolyte) after 1 and 24 h reaction times are essentially identical, indicating that adsorption is complete within 60 min (Fig. 1). The log–log scale isotherm exhibits characteristic features of anionic surfactant adsorption to positive-charged metal oxides as reported in the literature [5,8–10]. Adsorption increases linearly at low SDS equilibrium concentrations, with a steep slope that can be attributed to attractive electrostatic interactions between the anionic sulfonate head and the positively charged α-Fe_2O_3 surface, in addition to lateral hydrophobic interactions between alkyl chains. The slope of the isotherm decreases with further increasing SDS equilibrium concentration and eventually reaches a plateau (adsorption maximum) at ca. 3.3 μmol m^{-2}. The decrease in slope is attributed to the electrostatic repulsion that results from formation of an SDS bilayer on the mineral surface, and the resulting reversal in interfacial charge.

3.1.2. SDS adsorption envelopes

Adsorption of SDS to α-Fe_2O_3 was studied at the $[SDS]_{total}$ values of 0.1, 1.0, and 10.0 mM as a function of pH for 24 h reaction time. Adsorbed mass of SDS consistently decreased with increasing pH for all total SDS concentrations, and it approached zero at pH > 9 (Fig. 2). The dominant adsorption mechanisms between the SDS molecules and the hematite surface are thought to involve head group electrostatics and tail group lateral hydrophobic interactions [8]. Since electrostatic attraction is a prerequisite for the formation of a monolayer cluster on the hematite surface, head group adsorption, in turn, influences the extent of hydrophobic tail interaction. Therefore, with increasing pH, a decrease in OSO_3^- electrostatic attraction diminishes the opportunities for intermolecular hydrophobic stabilization at the solid/aqueous interface, resulting in greatly diminished sorption when pH exceeds the point of zero charge (pzc) of hematite (~pH 7.7–7.8).

3.1.3. Effects of SDS on hematite dissolution

Dissolution of α-Fe_2O_3 was assessed by measuring the Fe concentration of 0.2 μm filtrate at pH 6 as a function of $[SDS]_{eq}$ following the adsorption isotherm experiments (Fig. 3a). At pH 6,

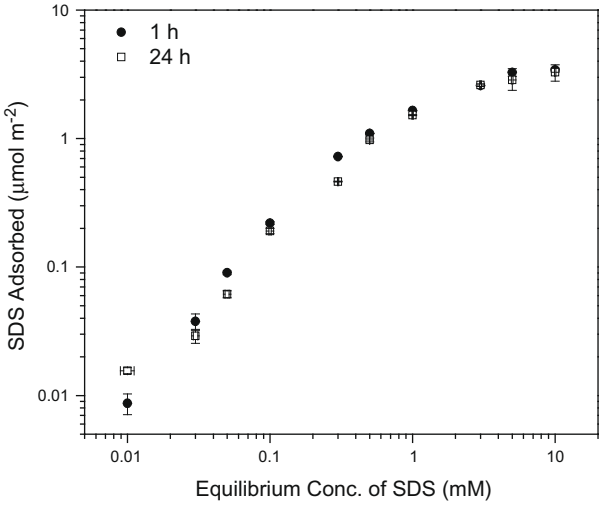

Fig. 1. Adsorption isotherms of SDS on α-Fe_2O_3 at pH 6.0 in 10.0 mM NaCl solution (5.0 g L^{-1} α-Fe_2O_3).

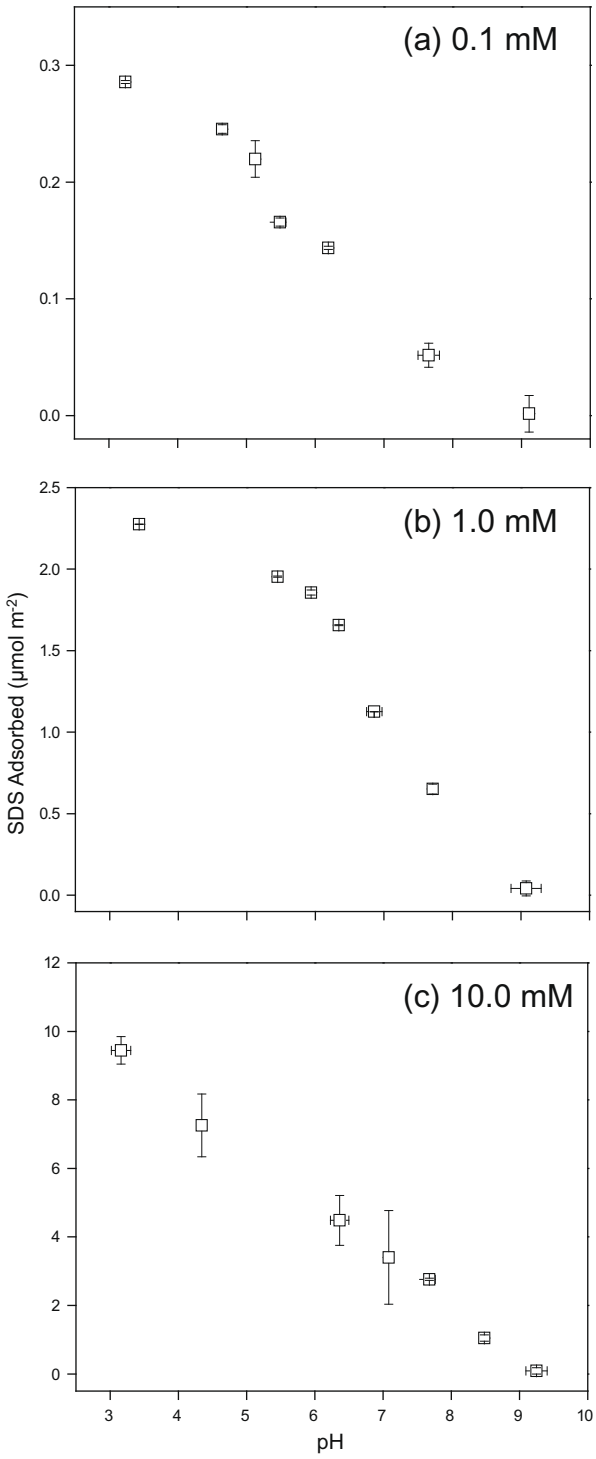

Fig. 2. SDS adsorption envelopes on α-Fe_2O_3 (24 h reaction time) at the SDS concentrations of (a) 0.1 mM, (b) 1.0 mM, and (c) 10.0 mM.

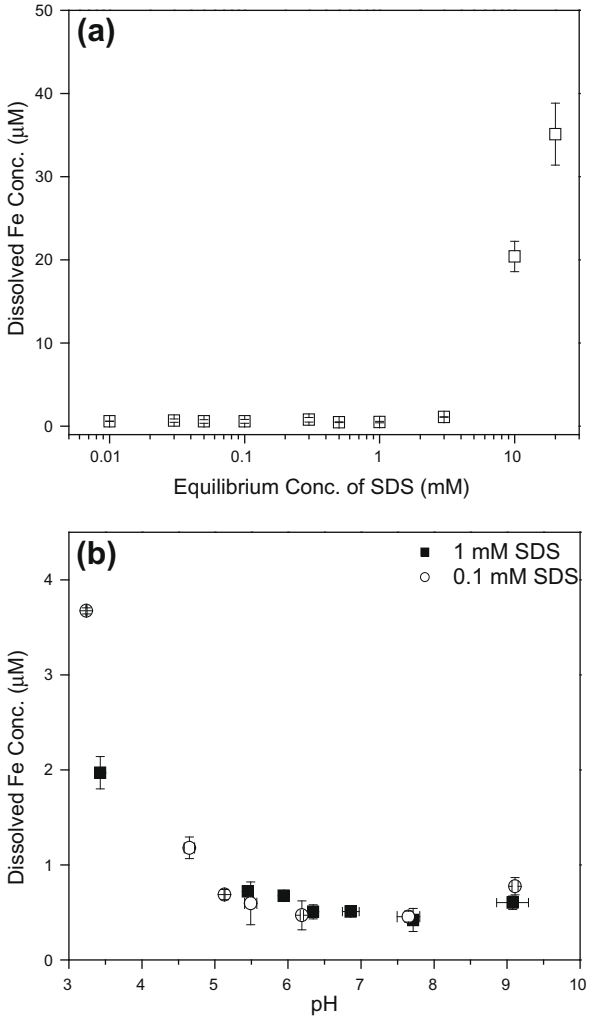

Fig. 3. Hematite dissolution rate (24 h reaction time) as a function of (a) SDS concentration at pH 6, and (b) pH in the presence of 0.1 and 1.0 mM SDS.

dissolution is low and independent of $[SDS]_{eq} < 3$ mM, indicating the lack of ligand-promoted hematite dissolution by SDS. However, we observed a significant increase in filtrate Fe as measured by ICP–MS above the cmc (Fig. 3a). We attribute this "threshold" Fe release to dispersion of nanocolloidal α-Fe_2O_3 upon formation of a complete SDS bilayer and associated surface charge reversal. That is, electrostatic repulsion between negatively charged surface bilayers apparently disperses the 10 to 20 nm diameter hematite colloids such that a portion of them are able to pass through the 0.2 μm filter. These dispersed nanoparticles are, therefore, measured by ICP–MS.

The effect of pH on hematite 24 h dissolution in the presence of variable SDS concentration is shown in Fig. 3b. While α-Fe_2O_3 dissolution exhibits well-known pH dependence (with minimum values close to the hematite pzc), effects of varying SDS concentration between 0.1 and 1 mM are minimal. The small effect of SDS on hematite dissolution in our experiments agrees with prior work that likewise showed negligible ligand-promoted dissolution effects of SDS. For example, Carrasco et al. [5] also showed that SDS did not promote hematite dissolution at low equilibrium concentration (<600 μM). These results are consistent with the formation of outer-sphere complexes between the charged sulfonate heads and the protonated hematite surface hydroxyl groups.

3.2. Infrared spectroscopy of SDS at ZnSe IRE and hematite surface

3.2.1. Adsorption mechanisms of SDS at solid/aqueous interfaces

Coating of the ZnSe ATR IRE with nanoparticulate hematite significantly increased the intensity of SDS IR absorptions. If hematite is absent from the ZnSe surface, intensities are at least 10-fold lower than those measured with the α-Fe_2O_3 coating (Fig. 4). Hence, under the experimental conditions, the presence of α-Fe_2O_3 nanoparticles significantly increased SDS retention within the aqueous sample region probed by the infrared evanescent wave. This wave

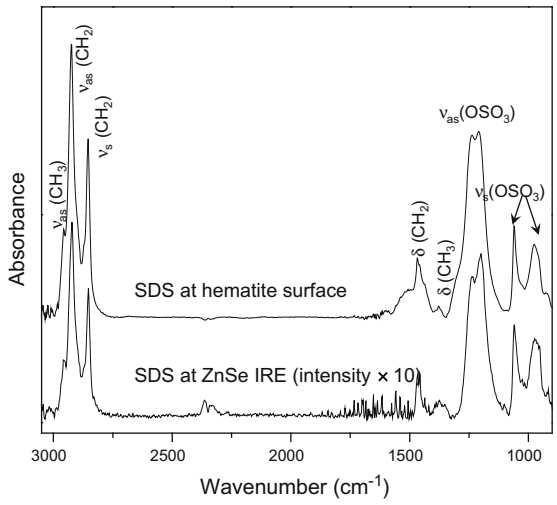

Fig. 4. ATR–FTIR spectra of SDS adsorbed to ZnSe IRE and α-Fe_2O_3 surface from 1.0 mM aqueous SDS solution at pH 6. The absorbance intensity of the spectrum at ZnSe IRE was increased 10 times for comparison.

extends into the sample to depths on the order of several hundred nm, with the precise distance depending on wavelength and refractive index of the aqueous suspension. The positive effect of hematite coating on SDS sorption to the IRE interface may, therefore, be attributable not only to the favorable charge properties of the Fe oxide, but also its effect on increasing the total area of mineral–water interface probed by the IR beam (Scheme 2). Besides the intensity difference, the spectra in Fig. 4 are almost identical, both containing two major spectral regions corresponding to the hydrophobic tail (3000–2800 cm^{-1}) and hydrophilic sulfonate head (1250–950 cm^{-1}), respectively.

In the 3000–2800 cm^{-1} region, the spectrum of SDS on the ZnSe IRE is dominated by the asymmetric and symmetric stretching bands of $-CH_3$ and $-CH_2-$ of the hydrocarbon tail [10,21,22]. The absorption band at 1461 cm^{-1} is due to the bending mode of $-CH_2-$, whereas the weak band at ~1377 cm^{-1} corresponds to a $-CH_3$ deformation. From 1250 to 950 cm^{-1}, the spectrum exhibits several distinct asymmetric and symmetric stretching bands of $-OSO_3^-$. The strong doublet at 1237 and 1200 cm^{-1} corresponds to asymmetric S–O stretching, whereas the peaks at 1060 and 974 cm^{-1} result from symmetric S–O stretching (see Table 1 for band assignments).

Table 1
Infrared absorption band assignments for SDS adsorbed to ZnSe IRE and α-Fe_2O_3 surface from 1 mM SDS aqueous solution at pH 6.

Wavenumber (cm^{-1})		IR band assignment
ZnSe	α-Fe_2O_3	
2957	2957	$\nu_{as}(CH_3)$
2921	2924	$\nu_{as}(CH_2)$
2873	2873	$\nu_s(CH_3)$
2852	2854	$\nu_s(CH_2)$
1461	1467	$\delta(CH_2)$
1373	1377	$\delta(CH_3)$
1237	1238	$\nu_{as}(OSO_3^-)$
1200	1208	$\nu_{as}(OSO_3^-)$
1060	1061	$\nu_s(OSO_3^-)$
974	976	$\nu_s(OSO_3^-)$

The correlation between symmetry and IR spectra of sulfate complexes has been well established [28]. The free aqueous SO_4^{2-} anion has tetrahedral symmetry (T_d), which exhibits an asymmetric, triply degenerate υ_3 band at 1102 cm^{-1}, in addition to the totally symmetric S–O stretching vibration at 980 cm^{-1} (υ_1) which is not IR active [18]. In the SDS structure, the symmetry of the sulfonate group is lowered from the T_d point group to the C_{3v} point group. As a consequence of the symmetry change, the υ_3 band of the asymmetric stretch splits into two bands: a doubly degenerate band at a higher wavenumber and a nondegenerate band at a lower wavenumber [18,28]. Since there is no electron orbital overlap, the symmetry of outer-sphere SDS complexes is similar to the free aqueous form, and no additional peaks emerge in the spectra. If SDS forms inner-sphere complexes at mineral surfaces, the symmetry of the terminal sulfonate group is expected to further reduce to C_{2v}, and the υ_3 band fully splits into three bands between 1250 and 1050 cm^{-1} [18]. The asymmetric stretching of sulfonate groups in the spectrum for the ZnSe IRE exhibits a doublet corresponding to C_{3v} symmetry, indicating no direct bond formation with the ZnSe surface.

The spectrum obtained from SDS adsorbed to the α-Fe_2O_3 surface shows features very similar to the spectrum at ZnSe IRE, indicating that the dominant adsorption mechanism involves outer-sphere complexation. This result is consistent with some prior studies [10,21,22]. The major difference occurs in the region of the asymmetric $-OSO_3^-$ stretch. As shown in Fig. 4 and Table 1, compared to the spectrum for SDS on ZnSe IRE, one of the $\nu_{as}(OSO_3^-)$ bands of the SDS spectrum on the α-Fe_2O_3 is shifted from 1200 to 1208 cm^{-1}, and the intensity of this band is

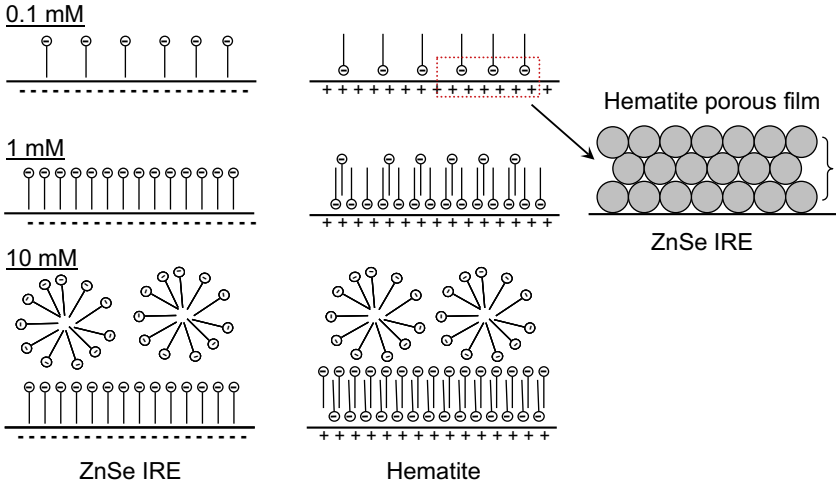

Scheme 2. SDS structures at ZnSe IRE and hematite interfaces at different SDS aqueous concentrations at pH 6.

diminished relative to the band at 1238 cm^{-1}. The two $\nu_{as}(OSO_3^-)$ bands correspond to a doubly degenerate E vibration and a second nondegenerate A vibration. As shown in Scheme 1, the directions of the transition dipole moment of the two vibrational modes are perpendicular to each other [23]. The A vibration at 1208 cm^{-1} is parallel to the SDS molecule and therefore is more sensitive to direct contact with charged surfaces, whereas the E vibrational mode at 1238 cm^{-1} is perpendicular to the SDS molecule and is sensitive to lateral surfactant–surfactant interactions [23]. Therefore, the change of the A mode $\nu_{as}(OSO_3^-)$ vibration observed in the spectrum results from a change in the local environment of the sulfonate head during adsorption at the α-Fe_2O_3 surface. A similar shift, observed for SDS adsorbed to Al_2O_3 and TiO_2, was attributed to H-bond formation between sulfonate head oxygen and mineral surface hydroxyls [21,22]. However, the same shift was observed at all pH values in our study (Table 2). Above the hematite pzc (at pH 9), the α-Fe_2O_3 surface is net negatively charged, which would be expected to diminish the probability of such H-bonding. An alternative explanation for the shift could be attributed to a change in SDS molecular structure and/or a change in dielectric constant of the interface in the presence of hematite. At the ZnSe IRE surface, in addition to electrostatic interactions, hydrophobic interactions between the hydrocarbon tail of the surfactant and the surface are expected to play a role in adsorption. Given the negative surface charge of the ZnSe surface (pzc ∼ pH 4) at the experimental pH and the greater hydrophobicity of ZnSe relative to α-Fe_2O_3 [29], it is plausible that SDS ions interact with the ZnSe surface largely through their hydrophobic tails, with the sulfonate head relegated to solution (Scheme 2). At the α-Fe_2O_3 surface, SDS likely has the opposite geometry with the first sorbate layer orienting the hydrophobic tail toward to the solution (Scheme 2). Therefore, we speculate that direct contact between the sulfonate head and the α-Fe_2O_3 surface results in the change of the A mode $\nu_{as}(OSO_3^-)$ vibration.

3.2.2. Effect of solution pH

Spectra for α-Fe_2O_3-sorbed SDS are shown as a function of pH and $[SDS]_{total}$ in Fig. 5. The spectra remain similar in structure across the pH range; no detectable peak shifts or emergent peaks are observed, but intensities are diminished with increasing pH when SDS concentrations are below the cmc (Fig. 5a and b). These results are consistent with the negative effect of pH on surface excess, as indicated by batch adsorption data (Fig. 2) and also with predominance of outer-sphere complexation. Below the SDS cmc and the hematite pzc, adsorption is dominated by electrostatic interactions between the negatively charged sulfonate head and the positively charged hematite surface hydroxyls. In contrast to the batch adsorption results, substantial FTIR signal remains even at pH 9.0 (above the pzc of α-Fe_2O_3), likely reflecting adsorption via Na^+ counterion bridging [30]. In addition, the porous hematite film present in the FTIR experiments, but not in the batch studies, could promote surface-induced formation of hemimicelles or admicelles well below the cmc in the film mesopores. Such an adsorption mechanism is expected to exhibit less pH dependency than isolated single SDS molecules adsorbed by attractive electrostatic forces, and may be responsible for the adsorption at pH 9 detected by FTIR.

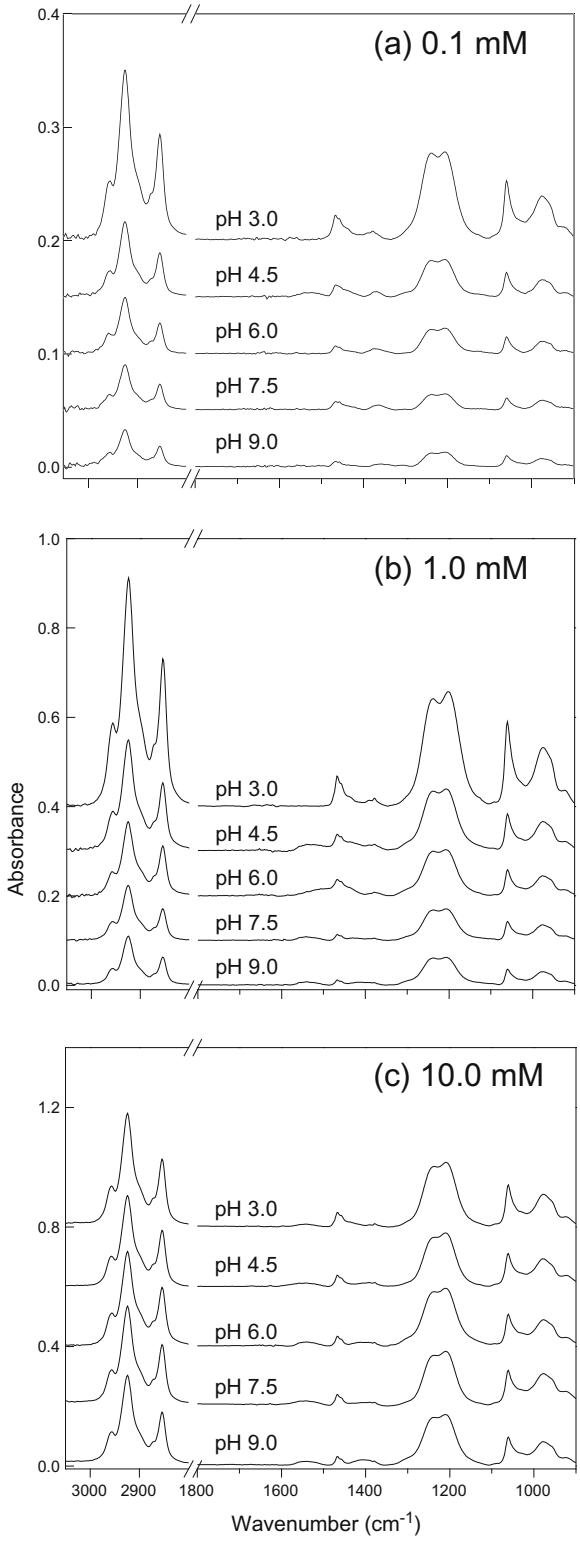

Fig. 5. ATR–FTIR spectra of SDS adsorbed to α-Fe_2O_3 as a function of pH at the SDS concentrations of (a) 0.1 mM, (b) 1.0 mM, and (c) 10.0 mM.

Table 2
Wavenumber (cm^{-1}) of the A vibrational mode of the $\nu_{as}(OSO_3^-)$ in the infrared spectra of SDS adsorbed to ZnSe IRE and α-Fe_2O_3 surface.

SDS concentration (mM)	ZnSe IRE			α-Fe_2O_3		
	pH 3	pH 6	pH 9	pH 3	pH 6	pH 9
0.1	1199	1198	1198	1206	1206	1206
1.0	1198	1200	1200	1202	1208	1208
10.0	1208	1208	1210	1210	1210	1210

At $[SDS]_{total}$ of 10 mM, which exceeds the cmc, IR spectra show a negligible response to solution pH across the range from 3 to 9 (Fig. 5c). This observation contrasts with the batch adsorption results (Fig. 2) that show diminished adsorption to the hematite

surface with increasing pH to 9. It also appears to contradict expectations based on SDS–hematite coulombic considerations, since micelles and hematite exhibit like charge at this pH. One possible explanation for this intriguing result is that under these particular conditions (pH > pzc and [SDS] > cmc), SDS micelles are weakly, but positively, adsorbed to the hematite surface via counterion bridging interactions. While weak nanoparticle–SDS micelle associations are expected to remain intact in the quiescent ATR cell, they could be disrupted via shear forces imposed during the centrifugation step required to measure surface excess in the batch experiments. In prior work, adsorption of anionic surfactant 4-C_{11}-paraxylene sulfonate to α- and γ-Al_2O_3 surfaces above the pzc was also observed, and was likewise attributed to counterion effects [30].

As shown in Fig. 6, the low wavenumber peak of the asymmetric doublet for $-OSO_3^-$ stretching shifts down in frequency (from 1208 to 1202 cm^{-1}) and becomes stronger relative to the higher wavenumber peak at 1238 cm^{-1} with decreasing pH in 1 mM SDS solution. A similar shift was previously reported by Bai et al. [10] at comparable SDS concentration (1.6 mM). Since the *A* vibrational mode of $-OSO_3^-$ is sensitive to direct contact with charged surfaces, and given that at pH 3, the α-Fe_2O_3 surface is populated with protonated surface hydroxyls, this shift could be attributed to H-bond formation between one or two sulfonate oxygens and surface $\equiv Fe–OH_2^+$ groups. The shift was not observed at either lower (i.e., 0.1 mM) or higher (i.e., 10 mM) SDS concentrations. We speculate that this is related to surfactant self-assembly at the solid/aqueous interface. That is, at intermediate SDS concentration, the formation of monolayer surface patches may induce changes in the local environment of the sulfonate head that enables partial dehydration of $-OSO_3^-$ ion and H-bond formation.

Similar to the spectral series for SDS at the α-Fe_2O_3 surface, that for the ZnSe IRE also shows strong negative pH dependence at low SDS concentrations (Fig. 7a and b) and negligible pH dependence at high concentration (Fig. 7c), albeit with much lower signal to noise, indicating lower interfacial adsorption overall. In contrast to the spectra for SDS on α-Fe_2O_3, no shift was detected for the A mode asymmetric stretching of the $-OSO_3^-$ group at pH 3 (Table 2), suggesting that SDS adsorption to the ZnSe IRE does not involve H-bonding of the sulfonate group. However, for spectra collected at 10 mM SDS, a noticeable change in the ratio of absorbance intensity of the hydrophobic tail relative to the sulfonate head was observed. As shown in Fig. 7c, the intensity ratio between $\nu_{as}(CH_2)$

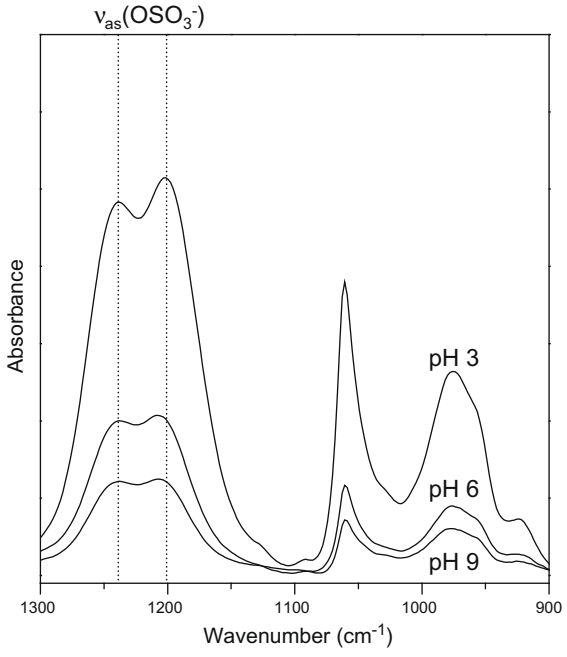

Fig. 6. ATR–FTIR spectra of SDS adsorbed to α-Fe_2O_3 (region 1300–900 cm^{-1}) at an SDS concentration of 1.0 mM.

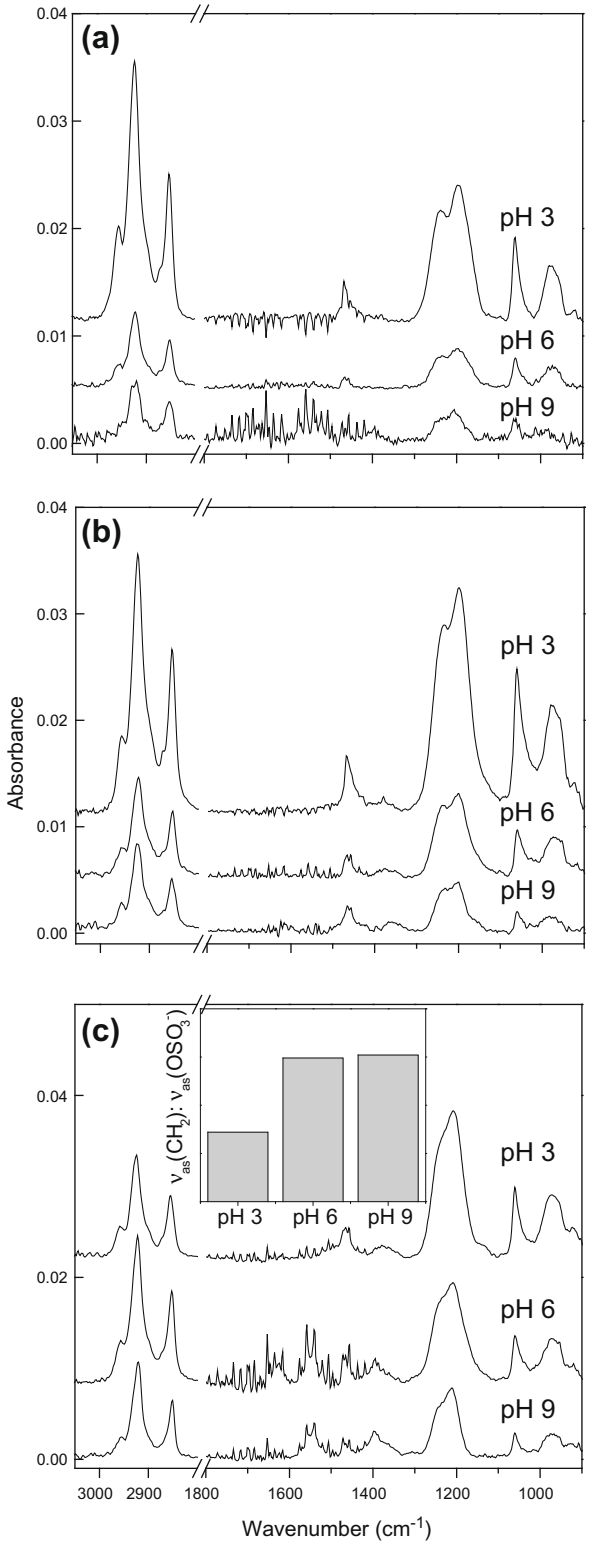

Fig. 7. ATR–FTIR spectra of SDS adsorbed to ZnSe IRE as function of pH at SDS concentrations of (a) 0.1 mM, (b) 1.0 mM, and (c) 10.0 mM. The insert in (c) is the peak area ratio between $\nu_{as}(CH_2)$ and $\nu_{as}(OSO_3^-)$.

and $\nu_{as}(OSO_3^-)$ increases with increasing pH. Such an effect was not detected in the SDS spectra when colloidal α-Fe_2O_3 was present (Fig. 5), since the intensity ratio in that case was essentially constant across the pH range.

We interpret this difference as resulting from the greater hydrophobicity and lower pzc (ca. pH 4) of the ZnSe IRE relative to hematite nanoparticles. Since the concentration is well above the surfactant cmc, SDS molecules are present as micelles in aqueous solution. As indicated in Scheme 3, the ZnSe IRE is positively charged at pH 3. Thus, it seems reasonable to expect that adsorption involves electrostatic attraction between the sulfonate head and the ZnSe surface, and the formation of a surficial bilayer. Conversely, when pH is greater than the pzc of ZnSe, the IRE is negatively charged, and like charge of the micelles and ZnSe diminishes adsorption at pH 6 and 9. However, even under these conditions, the hydrophobic surface may still serve as a suitable substrate for adsorption of the surfactant hydrophobic tail, forming a monolayer or more complex cylindrical hemimicelles [31] with the sulfonate head toward the solution (Scheme 3). Since ATR infrared spectra are biased toward moieties residing in closest proximity to the IRE surface, hydrophobic interactions between the ZnSe IRE surface and the SDS hydrocarbon chains may lead to an increase in the intensity ratio of $\nu_{as}(CH_2)$ and $\nu_{as}(OSO_3^-)$ at pH 6 and 9.

3.2.3. Effect of SDS concentration

It is well known that self-assembly can affect adsorption mechanisms and aggregate structure of surfactants at solid/aqueous interfaces [4,12]. To explore this effect spectroscopically, FTIR data were collected at the same SDS concentrations used in the batch adsorption envelope experiments (0.1, 1.0, and 10.0 mM). The spectra of SDS adsorbed to α-Fe_2O_3 at pH 6 are shown in Fig. 8. IR absorbance intensities increase consistently with increasing SDS concentration in a trend that is quantitatively consistent with batch uptake data (Fig. 8, inset). In both cases, the trend can be explained by surfactant self-association at the interface. At low concentrations, SDS ions are bound to the surface mainly by electrostatic attraction. Increasing surfactant concentration leads to the formation of monolayer or bilayer patches at the surface where sorbate–sorbate associations contribute to increased adsorption. Close inspection of the $-OSO_3^-$ stretching region (Fig. 9) shows that, as was observed with decreasing pH, and hence higher sorbate densities (Fig. 6), the intensity of the low frequency asymmetric stretching band at 1208 cm^{-1} is increased relative to that of the high frequency band at 1238 cm^{-1}. This spectral change should, therefore, be likewise attributable to changes in the local environment of the sulfonate head due to surfactant self-association at the hematite interface.

In contrast, SDS absorbance intensities (e.g., $\nu_{as}(OSO_3^-)$) on the ZnSe IRE do not show linear correlation with SDS concentration (Fig. 10). Peak intensities increase only slightly from 0.1 to 10.0 mM. As discussed above, the increase in adsorption to the α-Fe_2O_3 surface is due to the formation of surfactant bilayer patches at high concentrations (Scheme 2). Assuming that the major driving force for adsorption to the negatively charged ZnSe IRE is hydrophobic interactions between the hydrocarbon tail of SDS and the solid surface (Scheme 2), protrusion of the sulfonate head into solution would be expected to hinder self-assembly (e.g., bilayer formation) of the surfactant. While the increase in SDS peak vibrations from 0.1 to 1.0 mM is likely due to an increase in interfacial density, no such increase occurs between 1.0 and 10.0 mM concentration, suggesting saturation of the interface (Fig. 10).

The most distinct changes accompanying the increase in SDS concentration on the ZnSe IRE occur in the asymmetric stretching region of $-OSO_3^-$. The band intensity at 1200 cm^{-1} becomes stronger with increasing concentration relative to the 1237 cm^{-1} band. In addition, the band is shifted to a higher wavenumber (1212 cm^{-1}) at 10 mM concentration. The shift and intensity

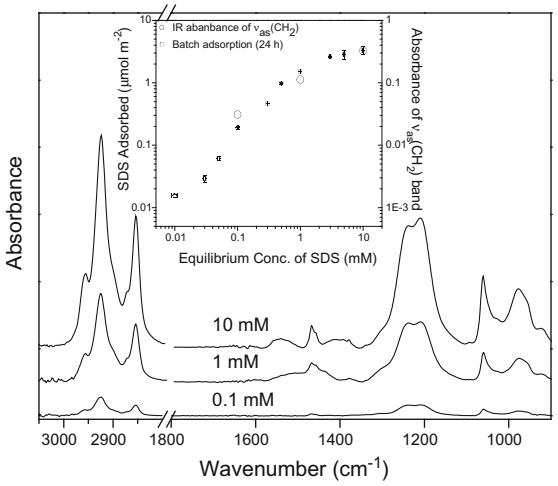

Fig. 8. ATR–FTIR spectra of SDS adsorbed to α-Fe_2O_3 as a function of SDS aqueous concentration at pH 6. The IR absorptions of the spectra (represented by the peak area of $\nu_{as}(CH_2)$) was plotted in the batch adsorption isotherm (24 h reaction time) in the insert.

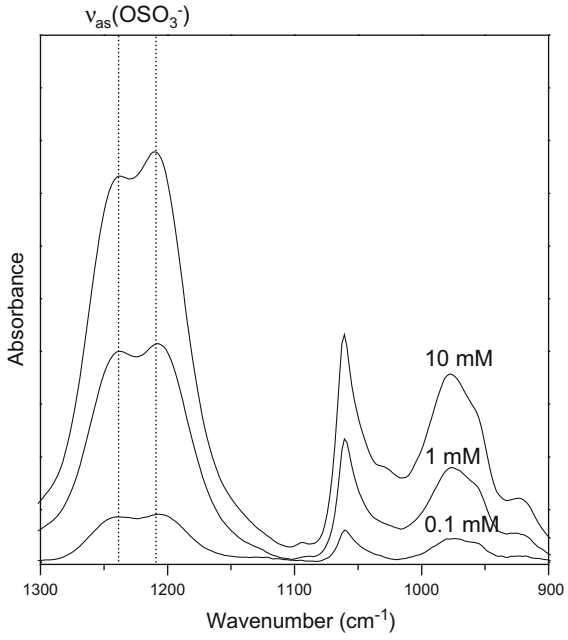

Fig. 9. ATR–FTIR spectra of SDS adsorbed to α-Fe_2O_3 (region 1300–900 cm^{-1}) at pH 6.

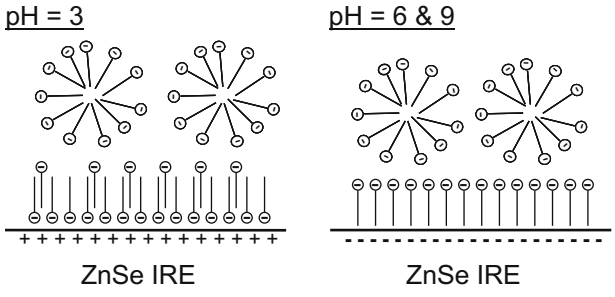

Scheme 3. SDS structures at ZnSe IRE interface at the concentration of 10 mM.

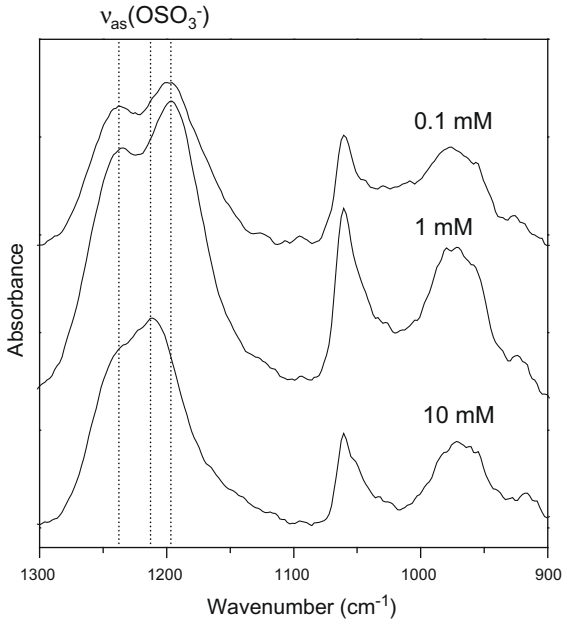

Fig. 10. ATR–FTIR spectra of SDS adsorbed to ZnSe IRE (region 1300–900 cm^{-1}) at pH 6.

increase of this band indicate an increased ordering or crowding of the sulfonate head group associated with aggregation and formation of micelles [32].

3.2.4. Kinetics of SDS adsorption

Time series of in situ ATR–FTIR spectra were collected from 0 min to 2 h for each system to assess the kinetics of SDS self-assembly at the ZnSe IRE and α-Fe_2O_3 surfaces as affected by aqueous solution chemistry. Since the bands of the asymmetric and symmetric stretching of $–CH_2–$ and $–CH_3$ groups do not shift significantly in response to changing solution chemistry and SDS concentration, the peak area of the asymmetric $–CH_2–$ stretch at ~2921 cm^{-1} (deconvoluted using GRAMS software) was used as a measure of SDS adsorption kinetics at the two interfaces [10].

Fig. 11a shows the time-dependent variation of SDS adsorption to the α-Fe_2O_3-coated IRE surface at pH 6. The absorbance of $\nu_{as}(CH_2)$ band increases slightly from 4 (the first spectrum collected) to 19 min, and remains constant thereafter for all SDS concentrations, indicating that surface uptake is a rapid process. The same time-dependent trend was observed for other pH values. Evidently, most adsorption occurs immediately after the introduction of the SDS solution and reaches equilibrium within 19 min. As discussed above, adsorption increases significantly with increasing SDS concentration due to surfactant self-assembly at the interface. The few studies that have previously examined kinetics of surfactant adsorption to charged particulate surfaces also reported rapid uptake that was completed within minutes [12,33]. Adsorption to α-Fe_2O_3 involves electrostatic attraction followed by formation of monolayer or bilayer (hemimicelle) patches at the mineral surface. A fluorescence spectroscopy study demonstrated SDS adsorption as monomers instead of complete micelles at the phosphatidylcholine liposome interface even above the cmc, which implies that the adsorption involves the initial breaking of the SDS micellar structure into monomers [34]. The disruption of micelles, driven by more favorable energetics of adsorption, could potentially limit uptake kinetics above the cmc. However, as shown in Fig. 11a, the time dependency of adsorption to α-Fe_2O_3 is similar above or below the cmc; in both cases, equilibrium is achieved within a few minutes.

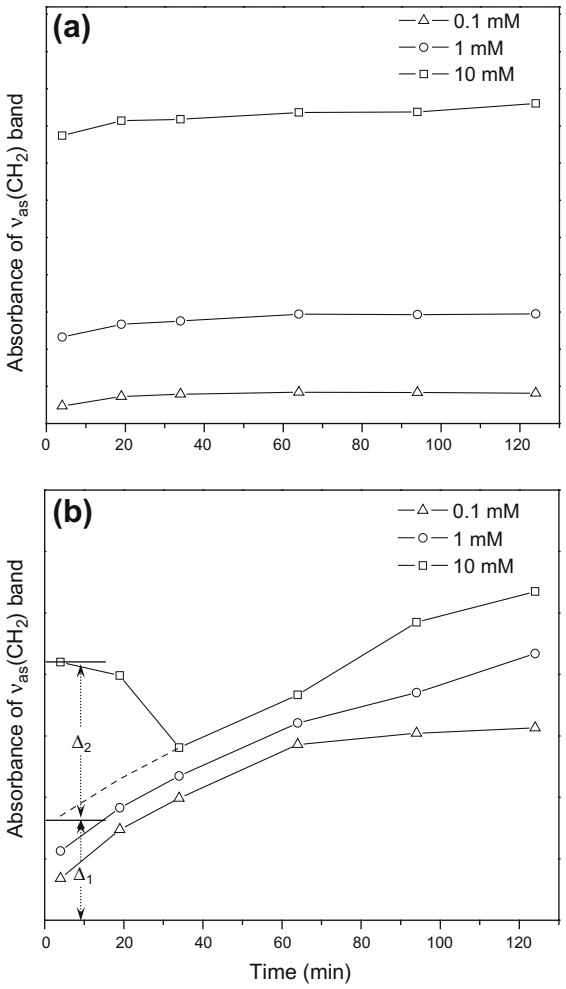

Fig. 11. Time dependence of SDS IR adsorption represented by the peak area of $\nu_{as}(CH_2)$ to (a) α-Fe_2O_3 surface and (b) ZnSe IRE at pH 6.

In contrast to rapid equilibration of SDS peak intensities at the α-Fe_2O_3 surface both above and below the cmc, IR spectra collected on the uncoated ZnSe IRE exhibit much stronger time dependence (Fig. 11b). In addition, there is only a slight increase in absorbance intensity as SDS concentration is increased from 0.1 to 10.0 mM. Below the cmc (i.e., for SDS concentrations of 0.1 and 1.0 mM), FTIR absorbance is initially small and increases progressively with reaction time due to an increase in amount of SDS mass sorbed to the surface. In so far as rapid adsorption to α-Fe_2O_3 at pH < pzc is facilitated by electrostatic attraction and subsequent surfactant self-assembly, the slower uptake to ZnSe IRE suggests mechanisms other than electrostatic interactions. The intercept indicated by Δ_1 in the figure represents the initial adsorption at 4 min, which probably results from weak electrostatic interactions (i.e., counter-ion effect) between the sulfonate head and the ZnSe surface. We attribute the further increase to hydrophobic interaction between the surfactant tail and the ZnSe IRE. Compared to favorable electrostatic interactions, the hydrophobic interaction and associated aggregate restructuring are weaker and, evidently, slower, reflecting the restricted motion of the C12 alkyl chains or a significant barrier for reorientation of SDS molecules at the hydrophobic ZnSe IRE surface [35].

However, when the initial SDS concentration is 10.0 mM, which is above the cmc, the adsorption shows a different trend. As shown in Fig. 11b, adsorbed mass decreases initially with time until a sorption minimum is reached at ~30 min, and then it increases

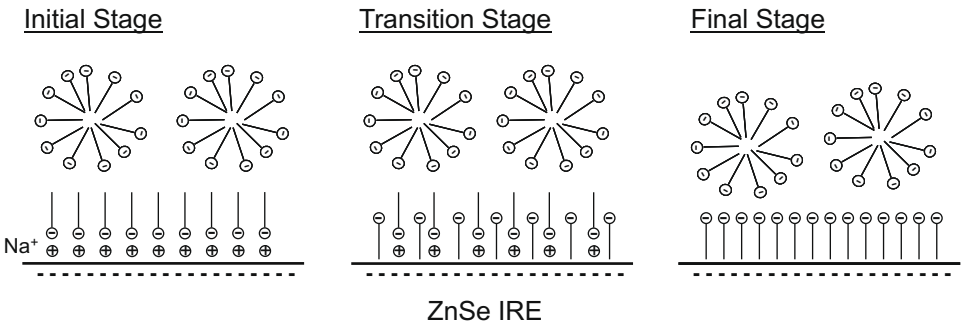

Scheme 4. SDS structures at ZnSe IRE interface at the concentration of 10 mM.

thereafter. Extrapolating the 10 mM SDS time trend from 30 to 4 min with the dashed line (Fig. 11b), adsorption exhibits very similar trends to the lower concentrations where initial adsorption (Δ_1) is postulated to be due to weak electrostatic interactions and further increase is thought to be due to the hydrophobic interactions. Thus, in addition to Δ_1, the further adsorbed mass indicated by Δ_2 results from interaction mechanisms that change with time. We propose the following explanation for the trend as an evolution of SDS structures at the solid/aqueous interface (Scheme 4). Rapid initial adsorption at higher [SDS] is driven by cation bridging between the charged sulfonate head and the ZnSe IRE. A transition to hydrophobic sorption occurs slowly, with the sulfonate head becoming oriented toward the solution. Hydrophobic interactions grow progressively with time and become dominant after 30 min. Aggregate restructuring via surfactant self-assembly (e.g., formation of interfacial hemimicelles) is a potential reason for the slow uptake kinetics on the more hydrophobic ZnSe IRE surface.

4. Conclusions

Adsorption of SDS was examined by combining ATR–FTIR spectroscopy with batch adsorption experiments across a range in pH and SDS concentration. Results indicate that SDS forms outer-sphere complexes at the α-Fe_2O_3 surface. The adsorption to ZnSe IRE involves both electrostatic attractive forces of the polar head group and hydrophobic interaction of the hydrocarbon tail with the IRE surface, whereas the adsorption to hematite is dominated by electrostatic interactions and surfactant self-assembly. As indicated by ATR–FTIR data, adsorption to both surfaces shows strong pH dependence at low SDS concentration and negligible pH dependence at [SDS] > cmc. The adsorption to α-Fe_2O_3 increases consistently with increasing SDS concentration due to the formation of monolayer or bilayer patches at the surface. In contrast, adsorption to ZnSe shows small variation with increasing concentration. Furthermore, the adsorption to the α-Fe_2O_3 surface appears to be a rapid process that reaches equilibrium within only a few minutes, whereas adsorption to the ZnSe IRE increases progressively with time, suggesting that the transition to hydrophobic sorption of the surfactant is a much slower process.

Acknowledgments

The authors thank Mary Kay Amistadi for the ICP-MS analysis. This research was funded by the US Department of Agriculture, National Research Initiative, Water and Watersheds Program (Grant 2006-35102-17192). We also thank two anonymous reviewers for helpful comments on the manuscript.

References

[1] A.A. Bodour, K.P. Drees, R.M. Maier, Appl. Environ. Microbiol. 69 (2003) 3280.
[2] D.B. Read, P.J. Gregory, New Phytol. 137 (1997) 623.
[3] S.D. Haigh, Sci. Total Environ. 185 (1996) 161.
[4] D.W. Fuerstenau, M. Colic, Colloids Surf., A 146 (1999) 33.
[5] N. Carrasco, R. Kretzschmar, M. Pesch, S.M. Kraemer, Environ. Sci. Technol. 41 (2007) 3633.
[6] N. Carrasco, R. Kretzschmar, M. Pesch, S.M. Kraemer, J. Colloid Interface Sci. 321 (2008) 279.
[7] L.K. Koopal, L. Keltjens, Colloids Surf. 17 (1986) 371.
[8] P. Chandar, P. Somasundaran, N.J. Turro, J. Colloid Interface Sci. 117 (1987) 31.
[9] M.R. Bohmer, L.K. Koopal, Langmuir 8 (1992) 2649.
[10] B. Bai, N.P. Hankins, M.J. Hey, S.W. Kingman, Ind. Eng. Chem. Res. 43 (2004) 5326.
[11] P. Somasundaran, D.W. Fuerstenau, J. Phys. Chem. 70 (1966) 90.
[12] R. Atkin, V.S.J. Craig, E.J. Wanless, S. Biggs, Adv. Colloid Interface Sci. 103 (2003) 219.
[13] Y. Ji, L. Black, R. Koster, M. Janek, Colloids Surf., A 298 (2007) 235.
[14] M. Almgren, S. Swarup, J. Colloid Interface Sci. 91 (1983) 256.
[15] W.A. Ducker, E.J. Wanless, Langmuir 15 (1999) 160.
[16] S.B. Velegol, B.D. Fleming, S. Biggs, E.J. Wanless, R.D. Tilton, Langmuir 16 (2000) 2548.
[17] P. Hansson, B. Jonsson, C. Strom, O. Soderman, J. Phys. Chem. B 104 (2000) 3496.
[18] S.J. Hug, J. Colloid Interface Sci. 188 (1997) 415.
[19] C.M. Eggleston, S. Hug, W. Stumm, B. Sulzberger, M.D.S. Afonso, Geochim. Cosmochim. Acta 62 (1998) 585.
[20] D. Peak, R.G. Ford, D.L. Sparks, J. Colloid Interface Sci. 218 (1999) 289.
[21] R.P. Sperline, Y. Song, H. Freiser, Langmuir 8 (1992) 2183.
[22] K.D. Dobson, A.D. Roddick-Lanzilotta, A.J. McQuillan, Vib. Spectrosc. 24 (2000) 287.
[23] H. Li, C.P. Tripp, J. Phys. Chem. B 108 (2004) 18318.
[24] J.S. Jeon, S. Raghavan, R.P. Sperline, Colloids Surf., A 92 (1994) 255.
[25] J. Shang, M. Flury, J.B. Harsh, R.L. Zollars, J. Colloid Interface Sci. 328 (2008) 299.
[26] U. Schwertmann, R.M. Cornell, Iron Oxides in the Laboratory: Preparation and Characterization, Wiley-VCH, Weinheim, Germany, 1991.
[27] X. Gao, D.W. Metge, C. Ray, R.W. Harvey, J. Chorover, Environ. Sci. Technol. 43 (2009) 7423.
[28] K. Nakamoto, Infrared and Raman Spectra of Inorganic and Coordination Compounds, Wiley, New York, 1986.
[29] S.J. Parikh, J. Chorover, Colloids Surf., B 62 (2008) 188.
[30] N.P. Hankins, J.H. O'Haver, J.H. Harwell, Ind. Eng. Chem. Res. 35 (1996) 2844.
[31] V.K. Paruchuri, A.V. Nguyen, J.D. Miller, Colloids Surf., A 250 (2004) 519.
[32] D.R. Scheuing, J.G. Weers, Langmuir 6 (1990) 665.
[33] R. Atkin, V.S.J. Craig, E.J. Wanless, S. Biggs, Langmuir 16 (2000) 9374.
[34] M. Cocera, O. Lopez, J. Estelrich, J.L. Parra, A. Maza, Langmuir 16 (2000) 4068.
[35] L.G. Olson, J.M. Harris, Appl. Spectrosc. 62 (2008) 149.